Parity violating elastic electron scattering and neutron density distributions in the relativistic Hartree-Bogoliubov model

Vretenar, Dario; Finelli, P.; Ventura, A.; Lalazissis, G. A.; Ring, Peter

Repository / Repozitorij:

Repository of the Faculty of Science - University of Zagreb

Parity violating elastic electron scattering and neutron density distributions in the relativistic Hartree-Bogoliubov model

D. Vretenar,[1,2,3] P. Finelli,[2] A. Ventura,[4] G. A. Lalazissis,[1,5,6] and P. Ring[1]

[1]*Physik-Department der Technischen Universität München, D-85748 Garching, Germany*
[2]*Physics Department, University of Bologna and INFN - Bologna, I-40126 Bologna, Italy*
[3]*Physics Department, Faculty of Science, University of Zagreb, 10 000 Zagreb, Croatia*
[4]*Centro Dati Nucleari, ENEA, Via Martiri di Monte Sole 4, and INFN - Bologna, I-40126 Bologna, Italy*
[5]*Wright Nuclear Structure Laboratory, Yale University, New Haven, Connecticut 06520*
[6]*Physics Department, Aristotle University of Thessaloniki, Thessaloniki GR-54006, Greece*

Parity-violating elastic electron scattering on neutron-rich nuclei is described in the framework of relativistic mean-field theory. Self-consistent ground state density distributions of Ne, Na, Ni, and Sn isotopes are calculated with the relativistic Hartree-Bogoliubov model, and the resulting neutron radii are compared with available experimental data. For the elastic scattering of 850 MeV electrons on these nuclei, the parity-violating asymmetry parameters are calculated using a relativistic optical model with inclusion of Coulomb distortion effects. The asymmetry parameters for chains of isotopes are compared, and their relation to the Fourier transforms of neutron densities is studied. It is shown that parity-violating asymmetries are sensitive not only to the formation of the neutron skin, but also to the shell effects of the neutron density distribution.

PACS number(s): 21.10.Gv, 21.60.$-$n, 25.30.Bf

I. INTRODUCTION

Measurements of ground state distributions of nucleons provide fundamental nuclear structure informations. The ground state densities reflect the basic properties of effective nuclear forces, and an accurate description of these distributions presents the primary goal of nuclear structure models.

Extremely accurate data on charge densities, and therefore on proton distributions in nuclei, are obtained from elastic scattering of electrons. Experimental data of comparable precision on neutron density distributions are, however, not available. It is much more difficult to measure the distribution of neutrons, though more recently accurate data on differences in radii of the neutron and proton density distributions have been obtained. Various experimental methods have been used, or suggested, for the determination of the neutron density in nuclei [1]. Among them, one that is also very interesting from the theoretical point of view, is parity-violating elastic electron scattering. In principle, the elastic scattering of longitudinally polarized electrons provides a direct and very accurate measurement of the neutron distribution. It has been shown that the parity-violating asymmetry parameter, defined as the difference between cross sections for the scattering of right- and left-handed longitudinally polarized electrons, produces direct information on the Fourier transform of the neutron density [2].

The possible use of parity-violating electron scattering from nucleons and nuclei to probe hadron structure and nuclear dynamics has been analyzed in many theoretical studies. The parity-violating asymmetry in elastic scattering of longitudinally polarized electrons from protons determines the anomalous baryon number magnetic moment [3]. The implications of strange-quark contribution to proton vector currents and their manifestation in parity-violating electron scattering experiments have also been analyzed in Ref.

[4]. The strange-vector current matrix element of the nucleon can also be extracted from the scattering of polarized electrons in an isoscalar nuclear magnetic transition [5]. Both the vector- and axial-vector-type strange quark current matrix elements of the nucleon can be studied in scattering of unpolarized electrons from a polarized target [6]. Additional aspects of parity-violating electron scattering studies of the strangeness content of the nucleon have been reviewed in Ref. [7].

Asymmetries of elastic electron scattering at low momentum transfer can be also used to study the difference of radii between neutron and proton distributions in nuclei. Suzuki [8] has shown that at low q the effects of the strangeness vector form factors of the nucleon ($q \lesssim 1.5$ fm^{-1}), and the effects of the charge form factor of the neutron ($q \lesssim 2.5$ fm^{-1}) on the asymmetry, are much smaller than those caused by the difference in the spatial extension of the neutron and proton densities. The asymmetries for elastic electron scattering ($q \lesssim 1$ fm^{-1}) on Ca, Sn, and Ba isotopes have been calculated in the plane wave approximation, and their mass number dependence has been related to the differences of radii between neutron and proton density distributions [9]. In a recent article [10], Horowitz has used a relativistic optical model to calculate the parity-violating asymmetry parameters for the elastic scattering of 850 MeV electrons on a number of spherical, doubly closed-shell nuclei. Ground state densities were calculated using a three-parameter Fermi formula and the relativistic mean-field model. Coulomb distortion corrections to the parity-violating asymmetry were calculated exactly. It has been shown that a parity violation experiment to measure the neutron density in a heavy nucleus is feasible.

Informations about the distribution of neutrons in nuclei should also constrain the isovector channel of the nuclear matter energy functional. A correct parametrization of the

isovector channel of effective nuclear forces is essential for the description of unique phenomena in exotic nuclei with extreme isospin values. For neutron-rich nuclei, these include the occurrence of nuclei with diffuse neutron densities, the formation of the neutron skin and the neutron halo. At the neutron drip-line different proton and neutron quadrupole deformations are expected, and these will give rise to low-energy isovector modes.

In the present work we describe parity-violating elastic electron scattering on neutron-rich nuclei in the framework of relativistic mean-field theory. The ground state density distributions will be calculated with the relativistic Hartree-Bogoliubov (RHB) model. This model represents a relativistic extension of the Hartree-Fock-Bogoliubov (HFB) framework, and it has been successfully applied in studies of the neutron halo phenomenon in light nuclei [11], properties of light nuclei near the neutron-drip line [12], ground state properties of Ni and Sn isotopes [13], the deformation and shape coexistence phenomena that result from the suppression of the spherical $N = 28$ shell gap in neutron-rich nuclei [14], the structure of proton-rich nuclei and the phenomenon of ground state proton emission [15–17]. In particular, it has been shown that neutron radii, calculated with the RHB model, are in excellent agreement with experimental data [12,13]. In studies of the structure of nuclei far from the β-stability line, both on the proton- and neutron-rich sides, it is important to use models that include a unified description of mean-field and pairing correlations [18]. For the ground state density distributions of neutron-rich nuclei in particular, the neutron Fermi level is found close to the particle continuum and the lowest particle-particle modes are embedded in the continuum. An accurate description of neutron densities can only be obtained with a correct treatment of the scattering of neutron pairs from bound states into the positive energy continuum.

Starting from the RHB self-consistent ground state neutron densities in isotope chains that also include neutron-rich nuclei, we will calculate the parity-violating asymmetry parameters for the elastic scattering of 850 MeV electrons. The main point in the present analysis will be to determine how sensitive the asymmetry parameters are to the variations of the neutron density distribution along an isotope chain. In this one respect our analysis presents an extension of the study reported in Ref. [9], where the parity-violating asymmetries for elastic electron scattering on several Ca, Sn, and Ba isotopes have been calculated in the plane wave approximation. However, as it has been shown in the recent extensive study of possible parity-violating measurements of neutron densities [19], by far the largest correction to the asymmetry comes from Coulomb distortions. For a heavy nucleus such as ^{208}Pb, Coulomb distortion effects can be of the order of 20%. Therefore, for any realistic comparison of parity-violating asymmetries with the Fourier transform of a neutron density, it is essential to include Coulomb distortion effects in the calculation of the elastic scattering cross section.

In addition to important information on nuclear structure, isovector interactions, the structure of neutron rich exotic nuclei, and neutron rich matter in astrophysics [19], neutron density measurements will be crucial for the analysis of atomic parity-violating (APV) experiments [19–21]. At the present level of APV experimental precision, the dominant inaccuracy in the interpretation of the data is associated with atomic theory uncertainties in the electron density at the nucleus. One possible way to circumvent these uncertainties is to measure APV observables for different atoms along an isotope chain [20]. In experiments involving isotope ratios, the atomic theory predictions largely cancel. On the other hand, such experiments will be very sensitive to changes in the neutron density distribution from one nucleus to the next along the isotope chain. This is because the parity-violating interaction is directly proportional to the overlap between electrons and neutrons. It would be therefore very important to be able to determine with high accuracy ($\approx 1\%$) the neutron spatial distribution for a sequence of isotopes. Moreover, for atomic PV experiments, and therefore for low-energy tests of the standard model, it would be ideal if the neutron density distribution were determined from the parity-violating elastic electron scattering on nuclei.

Another interesting question is whether parity-violating electron scattering could be used, in principle at least, to measure the neutron skin, or even the formation of the neutron halo. Of course, studies of electron scattering on stable or radioactive nuclei necessitate the operation of very complex experimental facilities. With the advent of high-quality electron beam facilities such as CEBAF, a precise measurement of neutron distribution in many stable nuclei through parity-violating electron scattering appears feasible [19]. The double storage ring MUSES, under construction at RIKEN, presents an interesting opportunity to study electron scattering on exotic radioactive nuclei. By injecting an electron beam, generated by a linear accelerator, in one of the storage rings, and storing a beam of unstable nuclei in the other, collision experiments between radioactive beams and electrons could be performed.

In Sec. II we present an outline of the relativistic Hartree-Bogoliubov model and calculate the self-consistent ground state neutron densities of Ne, Na, Ni, and Sn isotopes. For the elastic scattering of longitudinally polarized electrons on these nuclei, in Sec. III we use a relativistic optical model to calculate the parity-violating asymmetry parameters. Coulomb distortion corrections are included in the calculation, and the resulting asymmetries are related to the Fourier transforms of the neutron densities. The results are summarized in Sec. IV.

II. RELATIVISTIC HARTREE-BOGOLIUBOV DESCRIPTION OF GROUND STATE DENSITIES

In the framework of the relativistic Hartree-Bogoliubov model [15,22], the ground state of a nucleus $|\Phi\rangle$ is represented by the product of independent single-quasiparticle states. These states are eigenvectors of the generalized single-nucleon Hamiltonian which contains two average potentials: the self-consistent mean-field $\hat{\Gamma}$ which encloses all the long range particle-hole (ph) correlations, and a pairing field $\hat{\Delta}$ which sums up the particle-particle (pp) correlations. The single-quasiparticle equations result from the variation

of the energy functional with respect to the Hermitian density matrix ρ and the antisymmetric pairing tensor κ. The relativistic Hartree-Bogoliubov equations read

$$\begin{pmatrix} \hat{h}_D - m - \lambda & \hat{\Delta} \\ -\hat{\Delta}^* & -\hat{h}_D + m + \lambda \end{pmatrix} \begin{pmatrix} U_k(\mathbf{r}) \\ V_k(\mathbf{r}) \end{pmatrix} = E_k \begin{pmatrix} U_k(\mathbf{r}) \\ V_k(\mathbf{r}) \end{pmatrix}. \tag{1}$$

$\hat{h}_D$ is the single-nucleon Dirac Hamiltonian, m is the nucleon mass, and $\hat{\Delta}$ denotes the pairing field. The column vectors represent the quasiparticle spinors and E_k are the quasiparticle energies. The chemical potential λ has to be determined by the particle number subsidiary condition in order that the expectation value of the particle number operator in the ground state equals the number of nucleons.

The Hamiltonian $\hat{h}_D$ describes the dynamics of the relativistic mean-field model [23]: nucleons are described as point particles; the theory is fully Lorentz invariant; the nucleons move independently in the mean fields which originate from the nucleon-nucleon interaction. Conditions of causality and Lorentz invariance impose that the interaction is mediated by the exchange of pointlike effective mesons, which couple to the nucleons at local vertices: the isoscalar scalar σ meson, the isoscalar vector ω meson, and the isovector vector ρ meson. The single-nucleon Hamiltonian in the Hartree approximation reads

$$\hat{h}_D = -i\boldsymbol{\alpha} \cdot \nabla + \beta(m + g_\sigma \sigma(\mathbf{r})) + g_\omega \omega(\mathbf{r}) + g_\rho \tau_3 \rho_3(\mathbf{r})$$

$$+ e\frac{(1 - \tau_3)}{2} A(\mathbf{r}), \tag{2}$$

where σ, ω, and ρ denote the mean-field meson potentials. g_σ, g_ω, and g_ρ are the corresponding meson-nucleon coupling constants, and the photon field A accounts for the electromagnetic interaction. The meson potentials are determined self-consistently by the solutions of the corresponding Klein-Gordon equations. The source terms for these equations are sums of bilinear products of baryon amplitudes, calculated in the *no-sea* approximation.

The pairing field $\hat{\Delta}$ in the RHB single-quasiparticle equations (1) is defined

$$\Delta_{ab}(\mathbf{r},\mathbf{r}') = \frac{1}{2} \sum_{c,d} V_{abcd}(\mathbf{r},\mathbf{r}') \kappa_{cd}(\mathbf{r},\mathbf{r}'), \tag{3}$$

where a,b,c,d denote quantum numbers that specify the Dirac indices of the spinors, $V_{abcd}(\mathbf{r},\mathbf{r}')$ are matrix elements of a general two-body pairing interaction, and the pairing tensor is

$$\kappa_{cd}(\mathbf{r},\mathbf{r}') = \sum_{E_k>0} U^*_{ck}(\mathbf{r}) V_{dk}(\mathbf{r}'). \tag{4}$$

The input parameters of the RHB model are the coupling constants and the masses for the effective mean-field Hamiltonian, and the effective interaction in the pairing channel. In most applications we have used the NL3 set of meson

masses and meson-nucleon coupling constants [24] for the effective interaction in the particle-hole channel: $m = 939$ MeV, $m_\sigma = 508.194$ MeV, $m_\omega = 782.501$ MeV, $m_\rho = 763.0$ MeV, $g_\sigma = 10.217$, $g_2 = -10.431$ fm^{-1}, $g_3 = -28.885$, $g_\omega = 12.868$, and $g_\rho = 4.474$. Results of NL3 model calculations have been found in excellent agreement with experimental data, both for stable nuclei and for nuclei far away from the line of β-stability. The NL3 interaction will also be used in the present analysis of ground state neutron densities. For the pairing field we employ the pairing part of the Gogny interaction

$$V^{pp}(1,2) = \sum_{i=1,2} e^{-((\mathbf{r}_1 - \mathbf{r}_2)/\mu_i)^2} (W_i + B_i P^\sigma - H_i P^\tau$$

$$- M_i P^\sigma P^\tau), \tag{5}$$

with the set D1S [25] for the parameters μ_i, W_i, B_i, H_i, and M_i ($i = 1,2$). This force has been carefully adjusted to the pairing properties of finite nuclei all over the periodic table. In particular, the finite range of the Gogny force automatically guarantees a proper cutoff in momentum space. On the phenomenological level, the fact that we are using a nonrelativistic interaction in the pairing channel of a relativistic Hartree-Bogoliubov model, has no influence on the calculated ground state properties. A detailed discussion of this approximation can be found, for instance, in Ref. [15].

The ground state of a nucleus results from a self-consistent solution of the RHB single-quasiparticle equations (1). The iteration procedure is performed in the quasiparticle basis. A simple blocking prescription is used in the calculation of odd-proton and/or odd-neutron systems. The resulting eigenspectrum is transformed into the canonical basis of single-particle states, in which the RHB ground state takes the BCS form. The transformation determines the energies and occupation probabilities of the canonical states.

In Ref. [13] we have performed a detailed analysis of ground state properties of Ni ($28 \leq N \leq 50$) and Sn ($50 \leq N \leq 82$) nuclei in the framework of the RHB model. In a comparison with available experimental data, we have shown that the NL3 + Gogny D1S effective interaction provides an excellent description of binding energies, neutron separation energies, and proton and neutron rms radii, both for even and odd-A isotopes. The RHB model predicts a reduction of the spin-orbit potential with the increase of the number of neutrons. The resulting energy splittings between spin-orbit partners have been discussed, as well as pairing properties calculated with the finite range effective interaction in the pp channel. In Figs. 1 and 2 we plot the self-consistent ground state neutron densities for the even-A Ni ($30 \leq N \leq 48$) and Sn ($56 \leq N \leq 74$) isotopes. The density profiles display pronounced shell effects and a gradual increase of neutron radii. In the insets we include the corresponding differences between neutron and proton rms radii. For Ni, the value of $r_n - r_p$ increases from ≈ 0.03 fm for ^{58}Ni to 0.39 fm for ^{76}Ni. The neutron skin is less pronounced for the Sn isotopes: $r_n - r_p = 0.27$ fm for ^{124}Sn. In Fig. 3 the difference of the neutron and proton rms radii for Sn isotopes are compared with recent experimental data [26]. The experimental values result
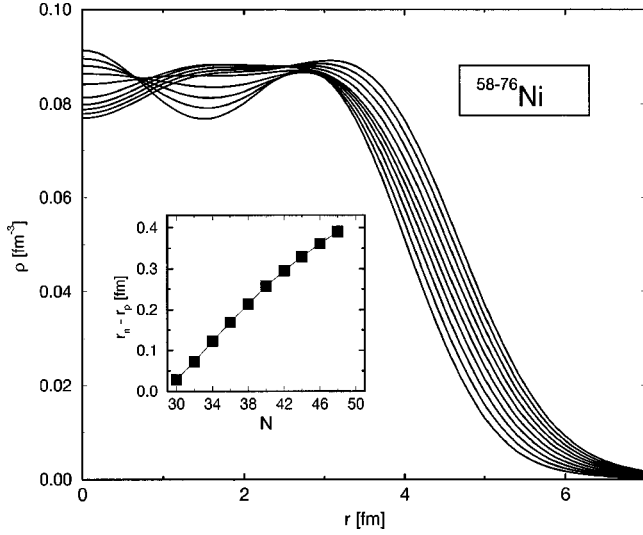
FIG. 1. Self-consistent RHB single-neutron density distributions for even-N Ni ($30 \leq N \leq 48$) nuclei, calculated with the NL3 + Gogny D1S effective interaction. The differences between neutron and proton rms radii are shown in the inset.
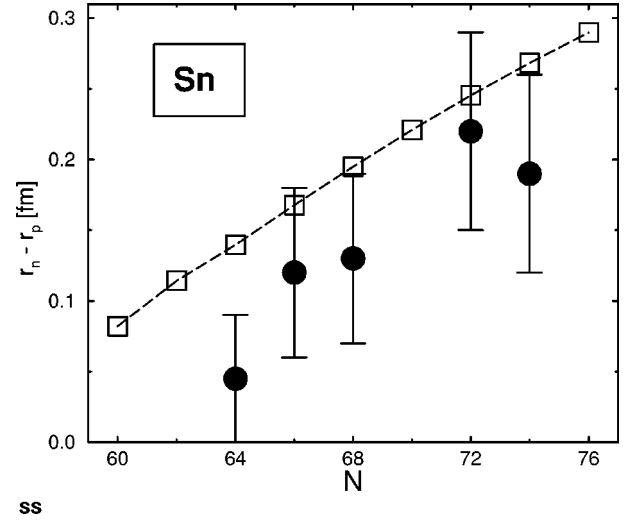

FIG. 3. Calculated differences between neutron and proton rms radii in Sn isotopes (squares), compared with experimental data from Ref. [26].

from measured cross sections of the isovector spin-dipole resonances in Sn nuclei. The agreement between theoretical and experimental values is very good. The calculated differences are slightly larger than the measured values, but they are still within the experimental error bars. This result, together with the analysis of Ref. [13], indicates that the ground state neutron densities of the Ni and Sn isotope chains are correctly described by the RHB model with the NL3 + Gogny D1S effective interaction.

The first experimental evidence of the formation of the neutron skin along a chain of stable and unstable isotopes was reported in Ref. [27] for the Na nuclei. By combining rms charge radii, determined from isotope-shift data, with interaction cross sections of Na isotopes on a carbon target, it has been shown that the neutron skin monotonically increases to 0.4 fm in neutron-rich β-unstable Na nuclei. In

Ref. [12] we have applied the RHB model in the description of properties of light nuclei with large neutron excess. The ground state properties of a number of neutron-rich nuclei have been analyzed: the location of the neutron drip-line, the reduction of the spin-orbit interaction, rms radii, changes in surface properties, and the formation of the neutron skin and the neutron halo. In particular, we have also calculated the chain of Na isotopes. The neutron density profiles are plotted in Fig. 4, with the differences of the neutron and proton rms radii in the insert. The calculations have been performed assuming spherical symmetry, i.e., deformations of proton and neutron densities were not taken into account. The blocking procedure has been used both for protons and neutrons. Strong shell effects are observed in the interior. In the central region the neutron density increases from ≈ 0.065 fm^{-3} for ^{26}Na, to more than 0.09 fm^{-3} for ^{27}Na. This effect, of

FIG. 2. Same as in Fig. 1, but for Sn isotopes ($56 \leq N \leq 74$).

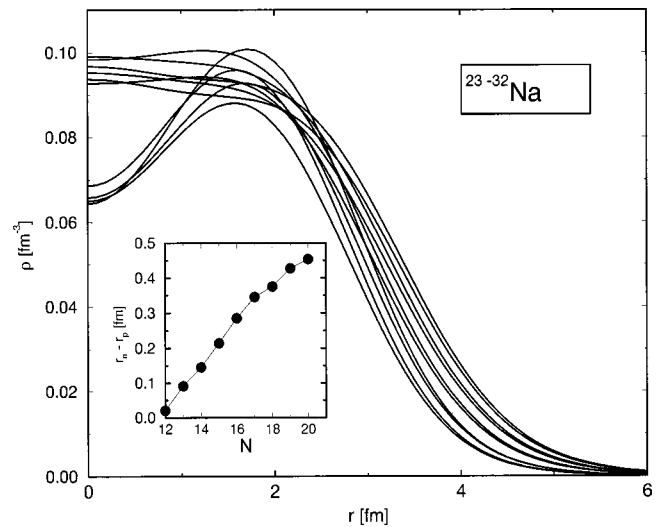
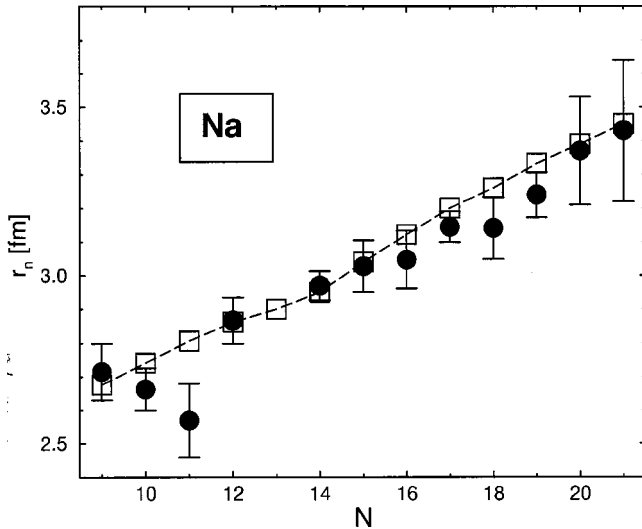FIG. 4. Self-consistent RHB single-neutron density distributions for Na ($12 \leq N \leq 21$) isotopes.

FIG. 5. Comparison of the calculated neutron rms radii for Na isotopes with experimental data from Ref. [27].

FIG. 6. Self-consistent RHB proton and neutron densities for ^{30,32,34}Ne.

course, corresponds to the filling of the $s\frac{1}{2}$ neutron orbital. At $r \approx 2$ fm the density decreases from 0.1 fm^{-3} to 0.09 fm^{-3}. The calculated neutron radii are compared with the experimental values [27] in Fig. 5. The model reproduces the trend of the experimental data and, with a possible exception of $N=11$, the theoretical values are in excellent agreement with the measured radii. The smooth increase of $r_n - r_p$ after $N=11$ (Fig. 4) is interpreted as the formation of the neutron skin. For $N=11$ the number of protons and neutrons is the same, and therefore both the odd proton and odd neutron occupy the $s-d$ orbitals with the same probabilities. An explicit proton-neutron short-range interaction, not included in our model, is probably responsible for a possible reduction of the neutron radius in this nucleus.

In some loosely bound systems at the drip lines, the neutron density distribution displays an extremely long tail: the neutron halo. The resulting large interaction cross sections have provided the first experimental evidence for halo nuclei [28]. The neutron halo phenomenon has been studied with a variety of theoretical models [29–31]. For very light nuclei in particular, models based on the separation into core plus valence space nucleons (three-body Borromean systems) have been employed. In Ref. [11] the RHB model has been applied in the study of the formation of the neutron halo in the mass region above the $s-d$ shell. Model calculations with the NL3 + Gogny D1S effective interaction predict the occurrence of neutron halo in heavier Ne isotopes. The study has shown that, in a mean-field description, the neutron halo and the stability against nucleon emission can only be explained with the inclusion of pairing correlations. Both the properties of single-particle states near the neutron Fermi level, and the pairing interaction, are important for the formation of the neutron halo. In Fig. 6 we plot the proton and neutron density distributions for ^{30}Ne, ^{32}Ne, and ^{34}Ne. The proton density profiles do not change with the number of neutrons. The neutron density distributions display an abrupt change between ^{30}Ne and ^{32}Ne. A long tail emerges, revealing the formation of a multiparticle halo. The formation of

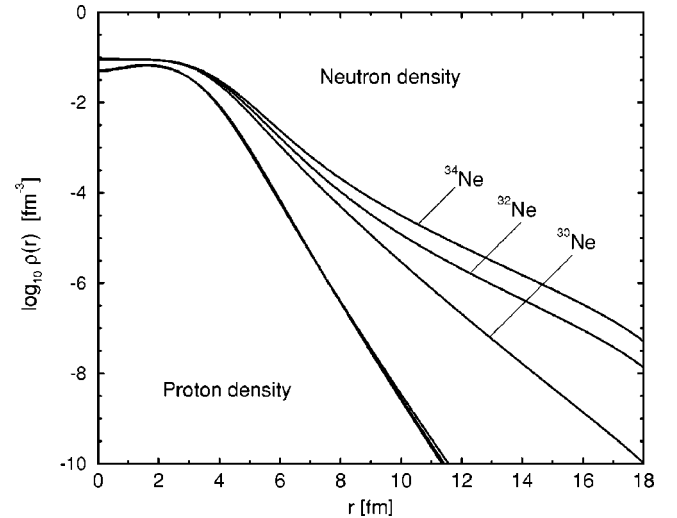the neutron halo is related to the quasidegeneracy of the triplet of states $1f_{7/2}$, $2p_{3/2}$, and $2p_{1/2}$. For $N \leq 22$ the triplet of states is in the continuum, it approaches zero energy at $N = 22$, and a gap is formed between these states and all other states in the continuum. The pairing interaction promotes neutrons from the $1f_{7/2}$ orbital to the $2p$ levels. Since these levels are so close in energy, the total binding energy does not change significantly. Due to their small centrifugal barrier, the $2p_{3/2}$ and $2p_{1/2}$ neutron orbitals form the halo.

III. PARITY VIOLATING ELASTIC ELECTRON SCATTERING

In this section we will illustrate how the neutron density distributions shown in Figs. 1–6 can be measured with polarized elastic electron scattering. We will calculate the parity-violating asymmetry parameter, defined as the difference between cross sections for the scattering of right- and left-handed longitudinally polarized electrons. This difference arises from the interference of one-photon and Z^0 exchange. As it has been shown in Ref. [2], the asymmetry in the parity-violating elastic polarized electron scattering represents an almost direct measurement of the Fourier transform of the neutron density.

The calculation procedure closely follows the derivation and definitions of Ref. [10]. We consider the elastic electron scattering on a spin-zero nucleus, i.e., on the potential

$$\hat{V}(r) = V(r) + \gamma_5 A(r), \tag{6}$$

where $V(r)$ is the Coulomb potential, and $A(r)$ results from the weak neutral current amplitude

$$A(r) = \frac{G_F}{2^{3/2}} \rho_W(r). \tag{7}$$

The weak charge density is defined

$$\rho_W(r) = \int d^3 r' G_E(|\mathbf{r} - \mathbf{r}'|)$$

$$\times [-\rho_n(r') + (1 - 4 \sin^2 \Theta_W) \rho_p(r')], \quad (8)$$

where ρ_n and ρ_p are point neutron and proton densities and the electric form factor of the proton is $G_E(r) \approx (\Lambda^3/8\pi) e^{-\Lambda r}$ with $\Lambda = 4.27$ fm^{-1}. $\sin^2 \Theta_W = 0.23$ for the Weinberg angle.

In the limit of vanishing electron mass, the electron spinor Ψ defines the helicity states

$$\Psi_{\pm} = \frac{1}{2}(1 \pm \gamma_5)\Psi, \quad (9)$$

which satisfy the Dirac equation

$$[\alpha \cdot \mathbf{p} + V_{\pm}(r)]\Psi_{\pm} = E\Psi_{\pm}, \quad (10)$$

with

$$V_{\pm}(r) = V(r) \pm A(r). \quad (11)$$

The parity-violating asymmetry A_l, or helicity asymmetry, is defined

$$A_l = \frac{d\sigma_+/d\Omega - d\sigma_-/d\Omega}{d\sigma_+/d\Omega + d\sigma_-/d\Omega}, \quad (12)$$

where $+(-)$ refers to the elastic scattering on the potential $V_{\pm}(r)$.

The calculation starts with the self-consistent relativistic Hartree-Bogoliubov ground state proton and neutron densities. The charge and weak densities are calculated by folding the point proton and neutron densities [see Eq. (8)]. The resulting Coulomb potential $V(r)$ and weak potential $A(r)$ (7) are used to construct $V_{\pm}(r)$. The cross sections for elastic electron scattering are obtained by summing up the phase shifts which result from the numerical solution of the partial wave Dirac equation. The calculation includes the Coulomb distortion effects. The cross sections for positive and negative helicity electron states are calculated, and the resulting asymmetry parameter A_l is plotted as a function of the scattering angle θ, or the momentum transfer q.

In order to check the correctness and accuracy of the computer code which calculates the elastic electron scattering cross sections, we have performed the same tests as those reported in Ref. [10]: experimental data are reproduced for the elastic cross sections from ^{208}Pb at 502 MeV [32]; plane wave approximation results are reproduced; it is verified that the asymmetry parameter A_l is linear in the potential $A(r)$ (7). We have also reproduced the parity-violating asymmetries calculated in Ref. [10]: elastic scattering at 850 MeV on ^{16}O, ^{48}Ca, and ^{208}Pb (relativistic mean-field densities), as well as on the three-parameter Fermi densities.

In Figs. 7 and 8 we plot the parity-violating asymmetry parameters A_l for the $^{58-76}$Ni isotopes, for the elastic electron scattering at 500 MeV and 850 MeV, respectively. The ground state neutron densities for these nuclei are shown in Fig. 1. For electron energies below 500 MeV the asymmetry
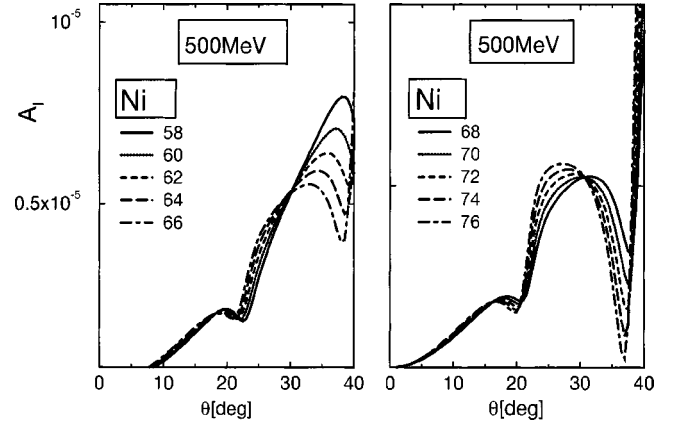

FIG. 7. Parity-violating asymmetry parameters A_l for elastic scattering from $^{58-76}$Ni at 500 MeV, as functions of the scattering angle θ.

parameters are small ($< 10^{-5}$), and the differences between neighboring isotopes are $< 10^{-6}$. At 850 MeV (the energy for which most of the calculations of Ref. [10] have been performed), the values of A_l are of the order of 10^{-5}. The differences between neighboring isotopes ($\approx 10^{-6}$) are especially pronounced for $^{58-66}$Ni, at $\theta \approx 20°$ and $\theta \approx 35°$. These differences reflect the strong shell effects calculated for the ground state neutron densities of the lighter Ni isotopes (see Fig. 1). The heavier Ni isotopes display more uniform neutron densities in the interior, and the resulting asymmetry parameters A_l are not very different. Similar results are also obtained at 1000 MeV electron energy. Of course, above 1 GeV the approximation of elastic scattering on continuous charge and weak densities is not valid any more, and the structure of individual nucleons becomes important. In the remainder of this section we show the results for A_l at 850 MeV electron energy. For all chains of isotopes we have also calculated the asymmetry parameters at 250 MeV, 500 MeV, and 1000 MeV. The energy dependence, however, is similar to that observed for the Ni isotopes: below 850 MeV the differences in the calculated A_l for the neighboring isotopes are too small.
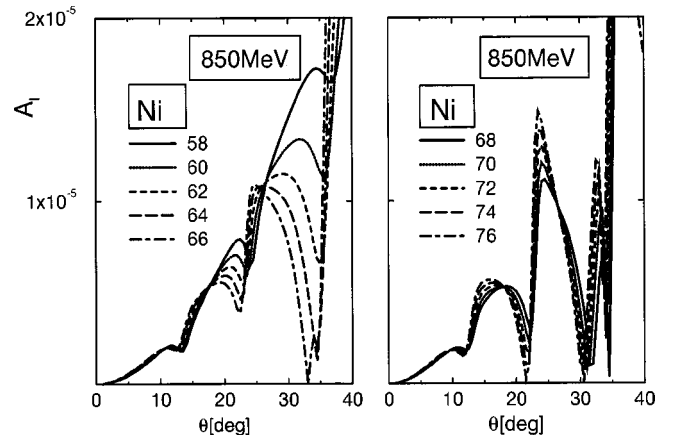

FIG. 8. Parity-violating asymmetry parameters A_l for elastic scattering from $^{58-76}$Ni at 850 MeV, as functions of the scattering angle θ.

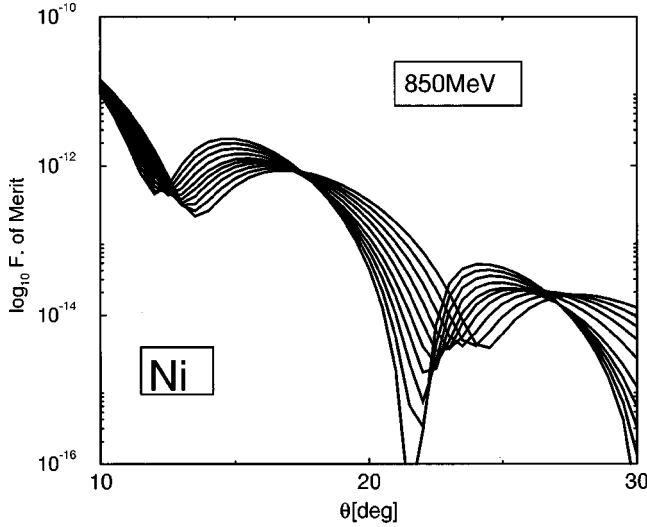FIG. 9. Figures of merit (13) as functions of the scattering angle θ, for elastic scattering from $^{58-76}$Ni at 850 MeV.

The figures of merit

$$F = A_l^2 \frac{d\sigma}{d\Omega}, \tag{13}$$

for 850 MeV electron scattering on the Ni isotopes are shown in Fig. 9. The figure of merit is, of course, strongly peaked at forward angles (see also Fig. 12 of Ref. [10]). In order to emphasize the differences between Ni isotopes, the F's are plotted in the interval $10° \leqslant \theta \leqslant 30°$. The figure of merit defines the optimal kinematics for an experiment in which the neutron density distribution could be determined from the measured parity-violating asymmetries.

The asymmetry parameter A_l provides a direct measurement of the Fourier transform of the neutron density [2]. In Figs. 10 and 11 we plot the asymmetries for the Ni isotopes
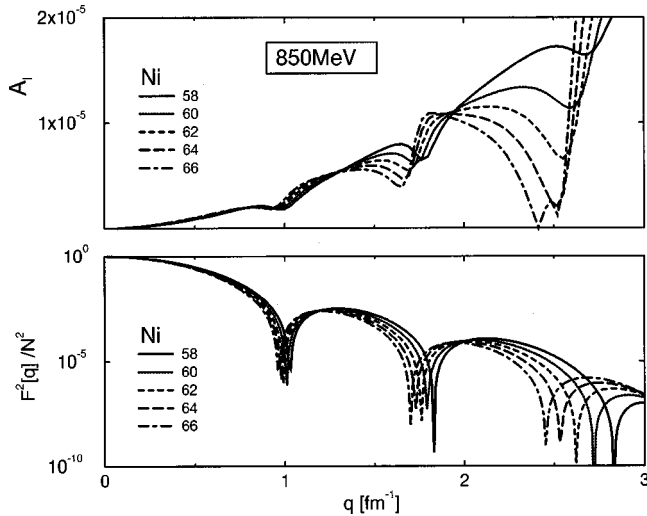

FIG. 10. Parity-violating asymmetry parameters A_l (upper panel) and squares of normalized Fourier transforms of neutron densities (lower panel), as functions of the momentum transfer q, for elastic scattering from $^{58-66}$Ni at 850 MeV.
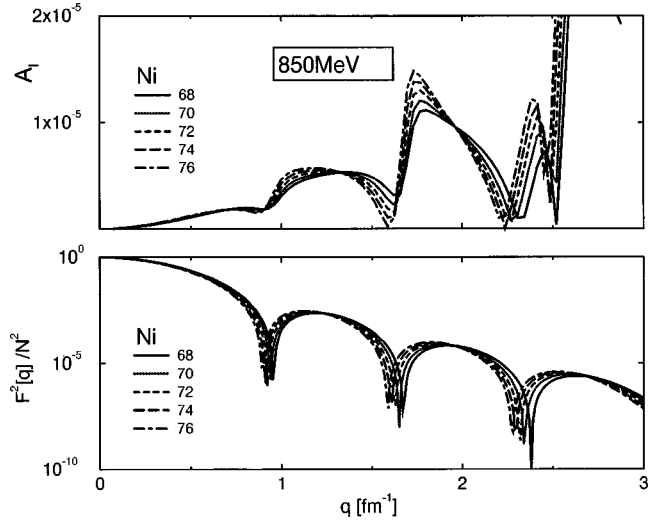

FIG. 11. Same as in Fig. 10, but for elastic scattering from $^{68-76}$Ni at 850 MeV.

(Fig. 8) as functions of the momentum transfer $q = 2E \sin\theta/2$, and compare them with the squares of the Fourier transforms of the neutron densities

$$F(q) = \frac{4\pi}{q} \int dr\, r^2 j_0(qr) \rho_n(r). \tag{14}$$

The differences between the asymmetries can be directly related to the form factors. Note that the positions of the minima of A_l correspond almost exactly to the minima of the form factors. Of course, the agreement would have been perfect if we had plotted the Fourier transforms of the weak density (8), but the differences are indeed very small. More important is the observation that the measurement of the parity-violating asymmetry at high momentum transfer might provide information about the details of the density profile of the neutron distribution.

In Fig. 3 we have shown that the differences in the neutron and proton rms radii, calculated with the RHB NL3 + Gogny D1S model, are in very good agreement with recent experimental data on Sn isotopes. In Fig. 12 we plot the asymmetry parameters A_l for the 850 MeV elastic electron scattering on the even $^{106-124}$Sn isotopes. The angular dependence is similar to that observed for the Ni nuclei; significant differences between neighboring isotopes are only found at $\theta > 20°$. The asymmetry parameters are compared to the Fourier transforms of the Sn neutron densities in Figs. 13 and 14.

The Na isotopes (Figs. 4 and 5) display the formation of the neutron skin, as well as strong shell effects in the central region of neutron densities. These shell effects are clearly seen in the plots of the asymmetry parameters A_l in Fig. 15. Especially pronounced is the transition between ^{26}Na and ^{27}Na, which corresponds to the filling of the $s\frac{1}{2}$ neutron orbital. The Fourier transforms of neutron densities are compared to the asymmetry parameters in Figs. 16 and 17. The differences between the minima of the asymmetry parameters for neighboring isotopes are the same as the differences
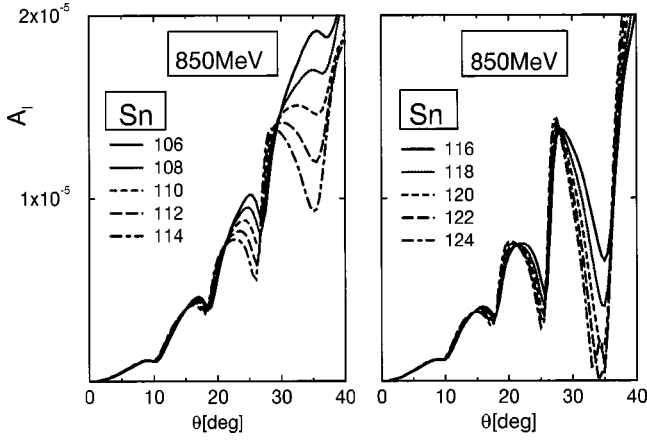
FIG. 12. Parity-violating asymmetry parameters A_l for elastic scattering from $^{106-124}$Sn at 850 MeV, as functions of the scattering angle θ.

between the minima of the Fourier transforms of the densities. In principle, it should be possible to deduce the neutron density distribution from the measured asymmetries.

An interesting theoretical question is whether the asymmetry parameters are sensitive to the formation of the neutron halo, i.e., whether parity-violating electron scattering could be used to detect the formation of the halo. For the even Ne nuclei, the neutron halo phenomenon is illustrated in Fig. 6. The tail in the neutron density develops in ^{32}Ne. The Fourier transforms of neutron densities and the asymmetry parameters A_l are shown in Fig. 18. At small momentum transfer the differences in the asymmetry parameters are very small. Only at $q \approx 2.5$ fm^{-1} the differences are of the order of 10^{-5}. This probably means that, even if it became possible to measure polarized elastic electron scattering on extremely neutron-rich nuclei, the parity-violating asymmetries would not be sensitive to the formation of the neutron halo.
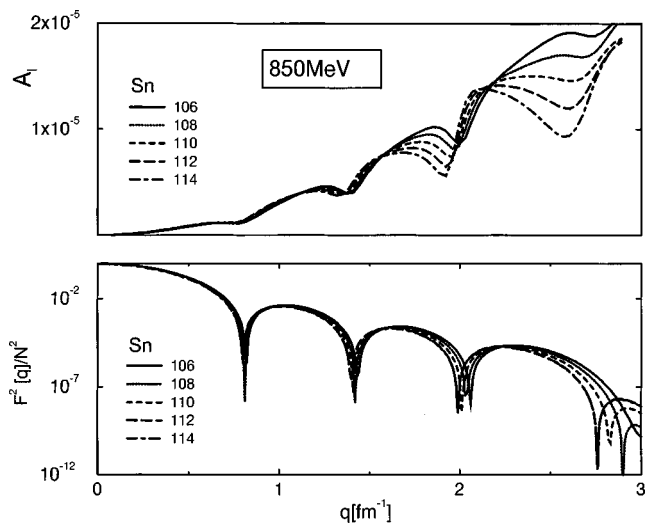

FIG. 13. Parity-violating asymmetry parameters A_l (upper panel) and squares of normalized Fourier transforms of neutron densities (lower panel), as functions of the momentum transfer q, for elastic scattering from $^{106-114}$Sn at 850 MeV.
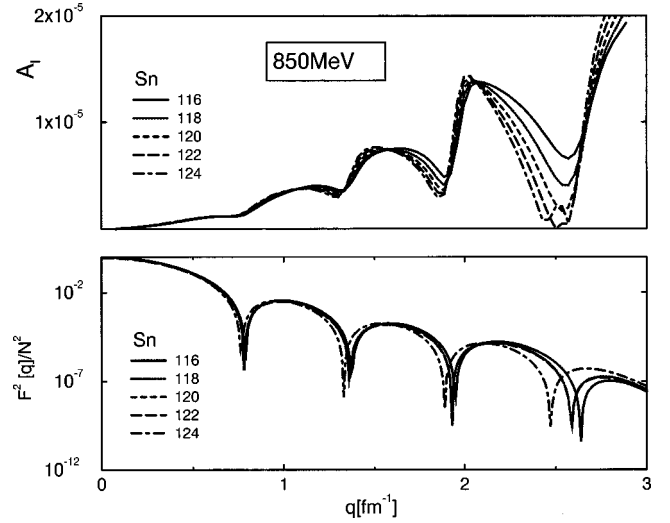

FIG. 14. Same as in Fig. 13, but for elastic scattering from $^{116-124}$Sn at 850 MeV.

IV. CONCLUSIONS

The relativistic mean-field theory has been used to study the parity-violating elastic electron scattering on neutron-rich nuclei. The parity-violating asymmetry parameter, defined as the difference between cross sections for the scattering of right- and left-handed longitudinally polarized electrons, provides direct information about the neutron density distribution.

The ground state neutron densities of neutron-rich Ne, Na, Ni, and Sn have been calculated with the relativistic Hartree-Bogoliubov model. The NL3 effective interaction has been used for the mean-field Lagrangian, and pairing correlations have been described by the pairing part of the finite range Gogny interaction D1S. The NL3 + Gogny D1S interaction produces results in excellent agreement with experimental data, not only for spherical and deformed β-stable nuclei, but
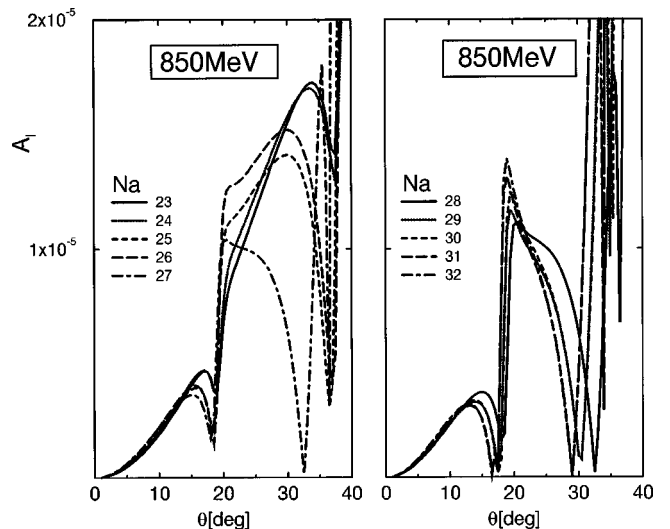

FIG. 15. Parity-violating asymmetry parameters A_l for elastic scattering from $^{23-32}$Na at 850 MeV, as functions of the scattering angle θ.
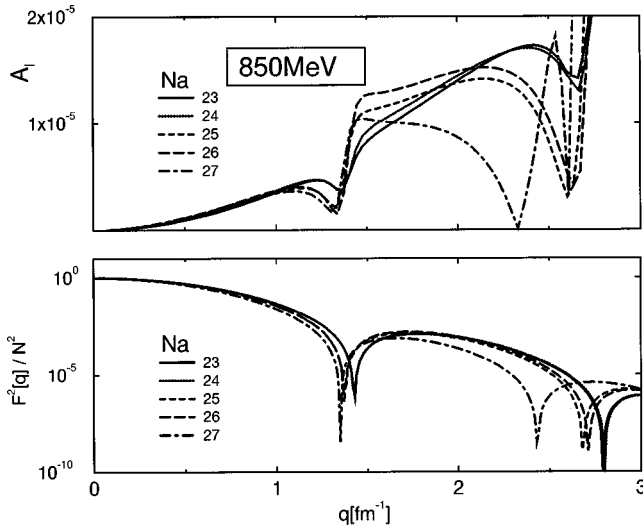
FIG. 16. Parity-violating asymmetry parameters A_l (upper panel) and squares of normalized Fourier transforms of neutron densities (lower panel), as functions of the momentum transfer q, for elastic scattering from $^{23-27}$Na at 850 MeV.

FIG. 18. Parity-violating asymmetry parameters A_l (upper panel) and squares of normalized Fourier transforms of neutron densities (lower panel), as functions of the momentum transfer q, for elastic scattering from ^{30,32,34}Ne at 850 MeV.

also for nuclear systems with large isospin values on both sides of the valley of β-stability. In the present work, in particular, the calculated neutron rms radii are shown to reproduce recent experimental data on Na and Sn isotopes.

Starting from the relativistic Hartree-Bogoliubov solutions for the self-consistent ground states, the charge and weak densities are calculated by folding the point proton and neutron densities. These densities define the Coulomb and weak potentials in the Dirac equation for the massless electron. The partial wave Dirac equation is solved with the inclusion of Coulomb distortion effects, and the cross sections for positive and negative helicity electron states are calculated. The parity-violating asymmetry parameters are plotted as functions of the scattering angle θ, or the momentum transfer q, and they are compared with the Fourier transforms
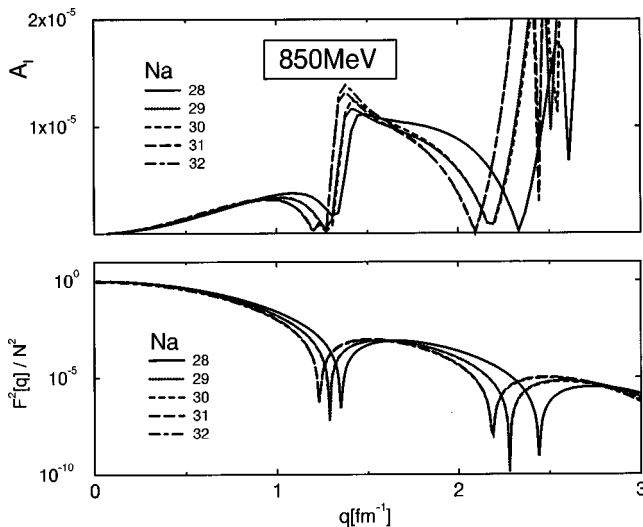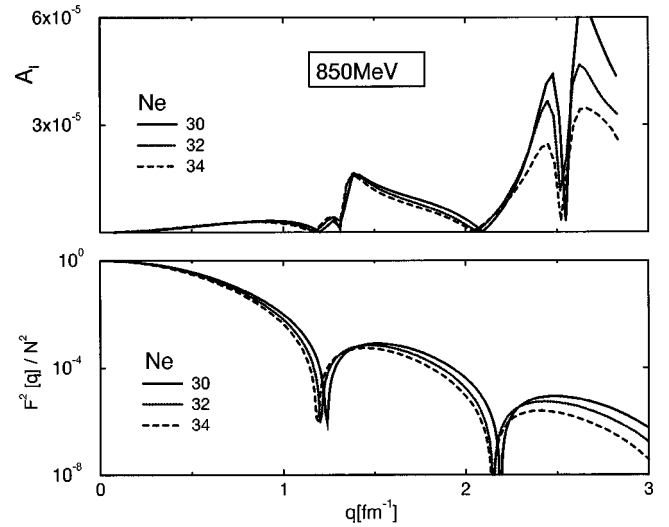
of the neutron density distributions.

We have compared the parity-violating asymmetry parameters for chains of neutron-rich isotopes. For low electron energies (≤ 500 MeV), the differences between neighboring isotopes are very small. At 850 MeV, significant differences in the parity-violating asymmetries are found at $\theta > 20°$. They can be related to the differences in the neutron density distributions. In particular, if plotted as function of the momentum transfer q, the asymmetry parameter can be related to the Fourier transform of the neutron density. It has been shown that the parity-violating elastic electron scattering is sensitive to the formation of the neutron skin in Na, Ni, and Sn isotopes, and also to the shell effects of the neutron density distributions. On the other hand, from the example of neutron-rich Ne nuclei, it appears that the asymmetry parameters would not be sensitive to the formation of the neutron halo.

Is there any possibility to actually measure the parity-violating asymmetries for the nuclei that we have considered in the present study? In a very recent study [19], Horowitz *et al.* have presented an extensive analysis of possible parity-violating measurements, their theoretical interpretation, and applications. In particular, future parity-violating measurements of neutron densities have been discussed. It appears that experiments on many stable nuclei are feasible at existing facilities. It has been shown that the theoretical corrections are either small or well understood, and therefore information on weak charge density, point neutron distributions and neutron density radii, can be directly extracted from experimental data. For instance, the CEBAF accelerator, with its high luminosity and remarkably stable electron beam, could be used to perform parity-violating elastic electron scattering experiments on many stable nuclei. The new physics sensitivity of a variety of low-energy parity-violating observables has been recently analyzed in Ref. [20]. It has been shown that a precise measurement of parity-violating asymmetries for electron-proton and electron-nucleus scat-

FIG. 17. Same as in Fig. 16, but for elastic scattering from $^{28-32}$Na at 850 MeV.

tering at Jefferson Laboratory is feasible. In particular, the importance of neutron density measurements in isotope chains for the analysis of atomic parity-violating (APV) experiments, and therefore for low-energy tests of the standard model, has been emphasized. Among the nuclei that we have considered in the present study, $^{58-64}$Ni and $^{112-124}$Sn are stable isotopes, and parity-violating elastic electron scattering experiments on these nuclei should be feasible at existing facilities. We note that the possibility to determine the difference of radii between proton and neutron distributions in Sn isotopes has been also discussed in Ref. [9]. Parity-violating measurements of neutron distributions in Sn nuclei could be compared with recent experimental data [26], obtained from measured cross sections of the isovector spin-dipole resonances. Measurements of parity-violating asymmetries in both Ni and Sn isotopes would provide important information on the isovector channel of the effective interactions.

The experimental situation is less clear for unstable nuclei. Studies of electron scattering on exotic radioactive nuclei will be possible at the double storage ring MUSES, presently under construction at RIKEN. The RI Beam Factory provides the possibility to store electron beams in one of the rings, and beams of unstable nuclei in the other ring. The expected luminosity for unstable nuclei is 10^{28-29} cm^2 sec, and it will be possible to determine the rms radii of a large number of unstable nuclei (600 nuclides). The measurement of parity-violating asymmetries is, of course, more difficult. We note that the available luminosity and short lifetimes might prevent the measurements at high-momentum transfer in the near future. However we conclude that, if it became possible to measure parity-violating elastic electron scattering on neutron-rich nuclei, the asymmetry parameters would provide detailed information on neutron density distributions, neutron radii, and differences between neutron and charge radii. This knowledge is, of course, essential for constraining the isovector channel of effective interactions in nuclei, and therefore for our understanding of the structure of nuclear systems far from the β-stability line.

ACKNOWLEDGMENTS

[1] C. J. Batty, E. Friedman, H. J. Gils, and H. Rebel, Adv. Nucl. Phys. **19**, 1 (1989).

[2] T. W. Donnelly, J. Dubach, and Ingo Sick, Nucl. Phys. **A503**, 589 (1989).

[3] R. D. McKeown, Phys. Lett. B **219**, 140 (1989).

[4] D. H. Beck, Phys. Rev. D **39**, 3248 (1989).

[5] T. Suzuki, Nucl. Phys. **A515**, 609 (1990).

[6] T. Suzuki, Phys. Rev. C **45**, 1939 (1992).

[7] M. J. Musolf, T. W. Donnelly, J. Dubach, S. J. Pollock, S. Kowalski, and E. J. Beise, Phys. Rep. **239**, 1 (1994).

[8] T. Suzuki, J. Phys. G **19**, 1319 (1993).

[9] T. Suzuki, Phys. Rev. C **50**, 2815 (1994).

[10] C. J. Horowitz, Phys. Rev. C **57**, 3430 (1998).

[11] W. Pöschl, D. Vretenar, G. A. Lalazissis, and P. Ring, Phys. Rev. Lett. **79**, 3841 (1997).

[12] G. A. Lalazissis, D. Vretenar, W. Pöschl, and P. Ring, Nucl. Phys. **A632**, 363 (1998).

[13] G. A. Lalazissis, D. Vretenar, and P. Ring, Phys. Rev. C **57**, 2294 (1998).

[14] G. A. Lalazissis, D. Vretenar, P. Ring, M. Stoitsov, and L. Robledo, Phys. Rev. C **60**, 014310 (1999).

[15] G. A. Lalazissis, D. Vretenar, and P. Ring, Nucl. Phys. **A650**, 133 (1999).

[16] D. Vretenar, G. A. Lalazissis, and P. Ring, Phys. Rev. Lett. **82**, 4595 (1999).

[17] G. A. Lalazissis, D. Vretenar, and P. Ring, Phys. Rev. C **60**, 051302 (1999).

[18] J. Dobaczewski, W. Nazarewicz, T. R. Werner, J. F. Berger, C. R. Chinn, and J. Dechargé, Phys. Rev. C **53**, 2809 (1996).

[19] C. J. Horowitz, S. J. Pollock, P. A. Souder, and R. Michaels, Los Alamos report nucl-th/9912038.

[20] M. J. Ramsey-Musolf, Phys. Rev. C **60**, 015501 (1999).

[21] S. J. Pollock and M. C. Welliver, Phys. Lett. B **464**, 177 (1999).

[22] P. Ring, Prog. Part. Nucl. Phys. **37**, 193 (1996).

[23] B. D. Serot and J. D. Walecka, Adv. Nucl. Phys. **16**, 1 (1986); Int. J. Mod. Phys. E **6**, 515 (1997).

[24] G. A. Lalazissis, J. König, and P. Ring, Phys. Rev. C **55**, 540 (1997).

[25] J. F. Berger, M. Girod, and D. Gogny, Nucl. Phys. **A428**, 32 (1984).

[26] A. Krasznahorkay *et al.*, Phys. Rev. Lett. **82**, 3216 (1999).

[27] T. Suzuki *et al.*, Phys. Rev. Lett. **75**, 3241 (1995).

[28] I. Tanihata *et al.*, Phys. Rev. Lett. **55**, 2676 (1985); Phys. Lett. B **206**, 592 (1988).

[29] I. Tanihata, Prog. Part. Nucl. Phys. **35**, 505 (1995).

[30] P. Hansen, A. S. Jensen, and B. Jonson, Annu. Rev. Nucl. Part. Sci. **45**, 591 (1995).

[31] J. Meng and P. Ring, Phys. Rev. Lett. **77**, 3963 (1996).

[32] B. Frois *et al.*, Phys. Rev. Lett. **38**, 152 (1977).